scientific reports

OPEN

Detectability and parameter estimation of stellar origin black hole binaries with next generation gravitational wave detectors

Mauro Pieroni[1]✉, Angelo Ricciardone[2,3] & Enrico Barausse[4,5,6]

We consider stellar-origin black hole binaries, which are among the main astrophysical sources for next generation gravitational wave (GW) detectors such as the Einstein Telescope (ET) and Cosmic Explorer (CE). Using population models calibrated with the most recent LIGO/Virgo results from O3b run, we show that ET and CE will be capable of detecting tens of thousands of such sources (and virtually all of those present in our past light cone up to $z \lesssim 0.7$ for ET and $z \lesssim 1$ for CE) with a signal-to-noise ratio up to several hundreds, irrespective of the detector design. When it comes to parameter estimation, we use a Fisher-matrix analysis to assess the impact of the design on the estimation of the intrinsic and extrinsic parameters. We find that the CE detector, consisting of two distinct L—shape interferometers, has better sky localization performance compared to ET in its triangular configuration. We also find that the network is typically capable of measuring the chirp mass, symmetric mass ratio and spins of the binary at order of 10^{-5}, 10^{-4} and 10^{-4} fractional error respectively. While the fractional errors for the extrinsic parameters are of order 10^{-2} for the sky localization, luminosity distance and inclination.

The European Strategy Forum on Research Infrastructures (ESFRI) has recently decided to include the Einstein Telescope (ET) gravitational wave (GW) detector in the 2021 roadmap[1,2]. At the same time the US community is planning to build the Cosmic Explorer (CE), a next generation GW detector with better sensitivity than existing LIGO/Virgo interferometers[3]. Together with LISA[4], this experimental effort is bound to revolutionize our understanding of the gravitational Universe. After the first detection of GWs by the LIGO/Virgo collaboration[5–8], nowadays the detection rate of binary black holes (BBHs) is around one per week. With next generation detectors, it is expected that ET at design sensitivity will perform around $\sim 10^5 - 10^6$ BBH detections and $\sim 7 \times 10^4$ binary neutron star (BNS) detections per year[9,10], i.e. up to several per hour. Moreover, given the one order of magnitude improvement in sensitivity compared to second generation interferometers, ET or CE will be able to detect BBHs and neutron star - black hole (NSBH) binaries with total mass between 20 and 100 $M_\odot$, up to redshift z $\sim$ 20. For BNS binaries (i.e. total masses $\sim 3M_\odot$), ET or CE should be able to reach $z \sim (2 - 3)$[11,12].

Such estimates are of course related to the detector configurations/positions and to the astrophysical population. At the time of writing, the final configuration and locations of ET and CE have not been yet decided. For ET, a triangular detector configuration seems the most plausible option. Concerning the location, at the moment there are two possibilities: one in Sardinia (Italy) and one in the Eusebio region of the Netherlands. On the US side, the shape of the CE interferometers should remain L-like, but characterized by longer arm-lengths (in particular, one interferometer of 40 km and one of 20 km).

The increased sensitivity of these detectors will have an impact on the parameter estimation accuracy, both for extrinsic and intrinsic source parameters. In this paper, we assess the detectability and the parameter estimation accuracy for one of the prime astrophysical sources for ET and CE, i.e, stellar-origin black hole binaries (SOBHBs). We build simulated populations of SOBHBs according to the latest mass functions inferred by LIGO/Virgo[13], and adopting the IMRPhenomXHM[14] waveform model, which includes higher order modes, and assumes quasi-circular (i.e. non-eccentric) and non-precessing black hole binaries. Then we use a Fisher matrix

[1]Blackett Laboratory, Imperial College London, South Kensington Campus, London SW7 2AZ, UK. [2]Dipartimento di Fisica e Astronomia "G. Galilei", Università degli Studi di Padova, via Marzolo 8, 35131 Padova, Italy. [3]INFN, Sezione di Padova, via Marzolo 8, 35131 Padova, Italy. [4]SISSA, Via Bonomea 265, 34136 Trieste, Italy. [5]INFN Sezione di Trieste, Trieste, Italy. [6]IFPU - Institute for Fundamental Physics of the Universe, Via Beirut 2, 34014 Trieste, Italy. ✉email: m.pieroni@imperial.ac.uk
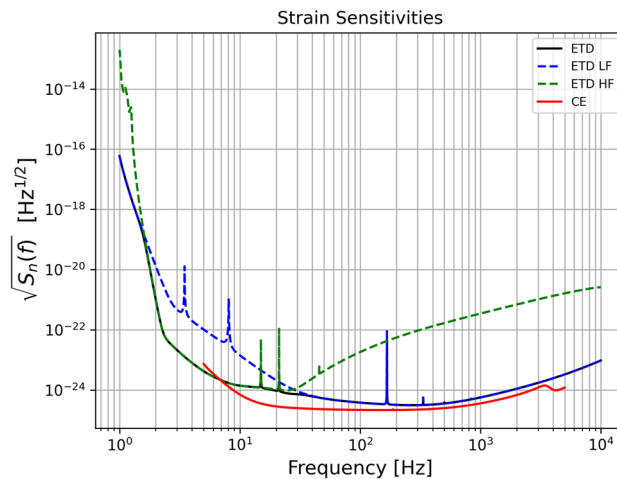
Figure 1. Plot of ET-D and CE strain sensitivities.

analysis to compare the accuracy in parameter estimation of the two detectors: one case where ET consists of three co-located nested detectors in a triangular configuration placed in Sardinia, and two hypothetical CE detectors consisting of two L-shaped interferometers placed one in Livingston and one in Hanford (where the two LIGO detectors are currently located).

We first estimate the number of observed sources as a function of redshift and total mass, both for ET and CE separately and for a network consisting of both detectors simultaneously, assuming a threshold in signal-to-noise ratio (SNR) of 20. We also comment on the horizon distance of these detectors, highlighting how the increase in this quantity relative to previous generation detectors will greatly enhance the discovery space also in 'exotic' regions of the parameter space (e.g. for putative black holes of sub-solar mass, which cannot be produced by stellar evolution and which could therefore be of primordial origin)[15–19].We also look at the distribution of the number of events and at the detected fraction of the astrophysical population, for the two detectors and the network, and we study the SNR distribution of the predicted detections.

We then move to the estimation of the errors on the source parameters, both intrinsic and extrinsic. Among the latter, we include the luminosity distance d_L, the sky localization Ω, the polarization angle ψ and the inclination angle ι. We quantify the fraction of events that can be detected with a sky location error smaller than 10, 1 and 0.1 square degrees, both at low ($z < 2$) and high redshift ($z > 2$). Similarly, we calculate the percentage of events that can be detected with a relative statistical error better than 20%, 10% and 5% on the luminosity distance. These estimates are relevant e.g. to project how GWs can potentially be used for investigating the large-scale structure (LSS) of the Universe[20–26], for studying the properties of the host galaxies[27] and for constraining cosmological parameters[28–31].

We also study the degradation of the luminosity distance estimates due to weak lensing, as a function of redshift. The latter acts as a systematic bias, which can influence astrophysical and cosmological parameter estimation[32–35].

Regarding the intrinsic source parameters, we derive projected errors on the chirp mass $\mathcal{M}_c$, the symmetric mass ratio η, the two spins $\chi_{1,2}$, again for ET and CE independently, and for a network of the two. For a selected event with large SNR in our simulated populations, we also present detailed Fisher Matrix posterior forecasts.

The structure of the paper is the following: in Sect. 3 we specify the assumed ET and CE detector properties, and we explain the procedure adopted for generating our simulated catalogues of sources; in Sect. 4 we present our parameter estimation results for the extrinsic and intrinsic parameters. A conclusion and an appendix on the adopted mass function and spin distribution for our simulated populations conclude the paper.

Detector characterization and catalogue generation
Detector properties.
ET and CE are next generation interferometers that will have an order of magnitude better sensitivity and a wider accessible frequency band (from 3 Hz to many kHz) than current GW detectors. The final configuration and the location of the detectors have not been finalized yet. However, in this paper, considering the most recent public specifications, we consider the most plausible case where ET consists of three co-located nested detectors in a triangular configuration placed in Sardinia. More in detail for ET each individual detector will be composed of two interferometers, one specialised for detecting low-frequency GWs and one for high-frequency GWs, forming a so-called xylophone configuration. The two interferometers will be of Michelson type with an opening angle of 60 degrees. Since the two detectors have a similar geometry, they will share common tunnels. As for the exact location, we consider the Sos Enattos mine in the city of Lula in Sardinia (N 40° 26′, E 9° 26′). For CE we consider the case of two L-shaped interferometers placed one in Livingston (N 30° 33′, W 90° 46′) and one in Hanford (N 46° 27′, W 119° 24′), where the two LIGO detectors are currently located. In the ET case, we consider a 10 km arm length, while for CE we consider 40 and 20 km respectively. We focus on the ET-D noise power spectral density[1,2], while for CE we consider that of[3,36]. In Fig. 1, we show the ET and CE strain sensitivities taken from[37]. For future reference, we also show the power law sensitivities[38,39] for sto-

chastic backgrounds, computed considering one year of mission and an SNR threshold of 10 for the background. In this study we do not consider networks that include current generation interferometers nor their upgraded A+ versions, but we just focus on next generation ones. The A+ detector generation will have an improvement in sensitivity of a factor ~ 2 to 4 depending on the frequency, compared to current generation detectors, driving the transition to next generation detectors such as ET and CE. For a detailed analysis including networks consisting also of A+ detectors, see[40].

Waveforms, astrophysical black hole populations and catalogue generation.   In our analysis we adopt the IMRPhenomXHM[14] waveform model, as implemented in PyCBC[41]. This waveform class includes higher order modes, and assumes quasi-circular (i.e. non-eccentric) and non-precessing black hole binaries, with $\chi_{1,2}$ the dimensionless spin parameters projected on the orbital angular momentum axis.

Overall, we therefore characterize our simulated black hole binaries by the following parameters:

$$z, \, m_1, \, m_2, \, \chi_1, \, \chi_2, \, \theta, \, \phi, \, \psi, \, \iota, \, \tau_c, \, \phi_0 \,, \tag{2.1}$$

where z is the redshift of the event, θ and ϕ are respectively the declination and right ascension of the source, ψ is the polarization angle, ι is the inclination angle, τ_c is the coalescence time and ϕ_0 is the initial phase of the binary. Below, we will perform a Fisher matrix analysis on these 11 parameters.

For a given detector, whose instrumental response can be characterized through the sky-dependent pattern functions $F_{ij}^{+/\times}$ (for the definition see for example[42]), the signal can be expressed as:

$$h = F_{ij}^+ h_{ij}^+ + F_{ij}^\times h_{ij}^\times \,. \tag{2.2}$$

The (optimal) SNR for a given source can then be computed as[43] *i.e.*

$$\mathrm{SNR}^2 = (h|h) \,, \tag{2.3}$$

where h is the waveform for the event, and $(a|b)$ denotes the noise weighted inner product:

$$(a|b) = 2 \int_{f_1}^{f_2} \frac{a(f)b^*(f) + a^*(f)b(f)}{S_n(f)} \, df \,, \tag{2.4}$$

where $S_n(f)$ is the detector strain sensitivity and f_1, f_2 are chosen to be the minimum and maximum frequencies of the detector's range.

We simulate catalogues of SOBHB systems by considering the latest population models from LIGO/Virgo O3*b* run[13] and the latest cosmological parameters constraints from[44]. In more detail, we consider a "power-law plus peak" mass function as described in the supplementary material, with a mass range $m_1, m_2 \in [2.3, 100.0]\, M_\odot$. For the spin distribution, we use the LIGO/Virgo *default* spin model that we summarize in the supplementary material. For the SOBHB merger rate, since ET and CE will reach large redshift, we have assumed that the merger rate tracks the Madau & Dickinson star formation rate as a function of redshift[45] convolving this with the time delay between the formation of the binary and its merger. For the time delay distribution we have considered an inverse power-law[40,46]

$$p(t_d) = \frac{1}{\ln\left(t_d^{\max}/t_d^{\min}\right) t_d} \,, \tag{2.5}$$

between $t_d^{\min} = 10\,Myr$ and $t_d^{\max} = 10\,\mathrm{Gyr}$. This means that the merger rate increases up to $z \sim 2$ and then decreases again at higher redshift. This dependence has also been considered in the LIGO/Virgo papers on the GW stochastic background[47]. We considered just one type of population of astrophysical objects (see[48] for an analysis which take into account different populations). The normalization of the merger rate is chosen such that its local value at $z = 0$ matches with the latest LIGO and Virgo observations (i.e., $R_0 = 17.3\,\mathrm{Gpc}^{-3}\mathrm{yr}^{-1}$, $k = 2.9$)[13]. We focus on the redshift interval $0 < z < 15$, but our results are insensitive to the maximum redshift that we consider. For simplicity, we do not consider the possibility of two or more overlapping signals and that we are able to identify all the events (techniques such as those employed in the LISA Data Challenge[39,49–51] may be beneficial to treat that case, or the inclusion of anisotropies could help[52]).

In terms of redshift reach, next generation detectors will be significantly better than LIGO/Virgo: comparing to the latter, which are sensitive to events up at redshift $z \lesssim 1$, ET and CE should reach up to $z \simeq 20$, depending on the mass[12], potentially probing the dark era of the Universe preceding the birth of the first stars, and opening the possibility to test a possible primordial origin for, at least part of, the BH population. In particular, in Fig. 2 we show the detector reach for equal mass, sky and inclination averaged binaries, in terms of the cosmological redshift, as a function of the source-frame total mass of the coalescing BHB and considering our default SNR threshold of 20. As can be seen, ET and CE can reach a similar redshift, however ET will be able to detect BHs with larger masses (up to $\sim 10^3 M_\odot$ up to $z \sim 10$). On the other hand, very small source-frame total mass sources (below $1 M_\odot$), which cannot be produced by stellar evolution and which could therefore point at the existence of primordial black holes, can be observed up to $z \approx .5$ (1) for ET (CE), if they exist.

Note that the large number of detected events by ET or CE, which we will show below to be of order 10^4 SOBHBs at high redshift and with a quite high SNR, will allow for gaining insight on stellar evolution and star formation (e.g. the impact of the metallicity)[53]. Besides this, the large statistics will also allow to use GW sources in combination with other cosmological probes like Large-Scale Structure (LSS), to shed light on formation scenarios[24,25], clustering properties[26,30,54], and test of General Relativity/Modified Gravity[34,55,56].
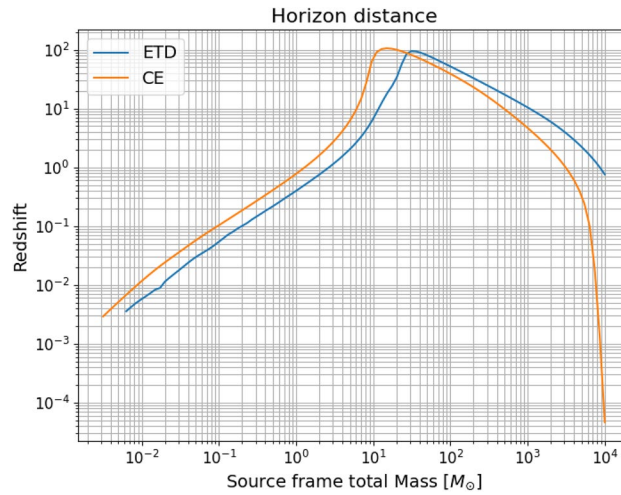
Figure 2. Horizon distance plot for ET and CE for equal mass system of black holes and assuming that all the events above $\mathrm{SNR}_{th} = 20$ are detectable.
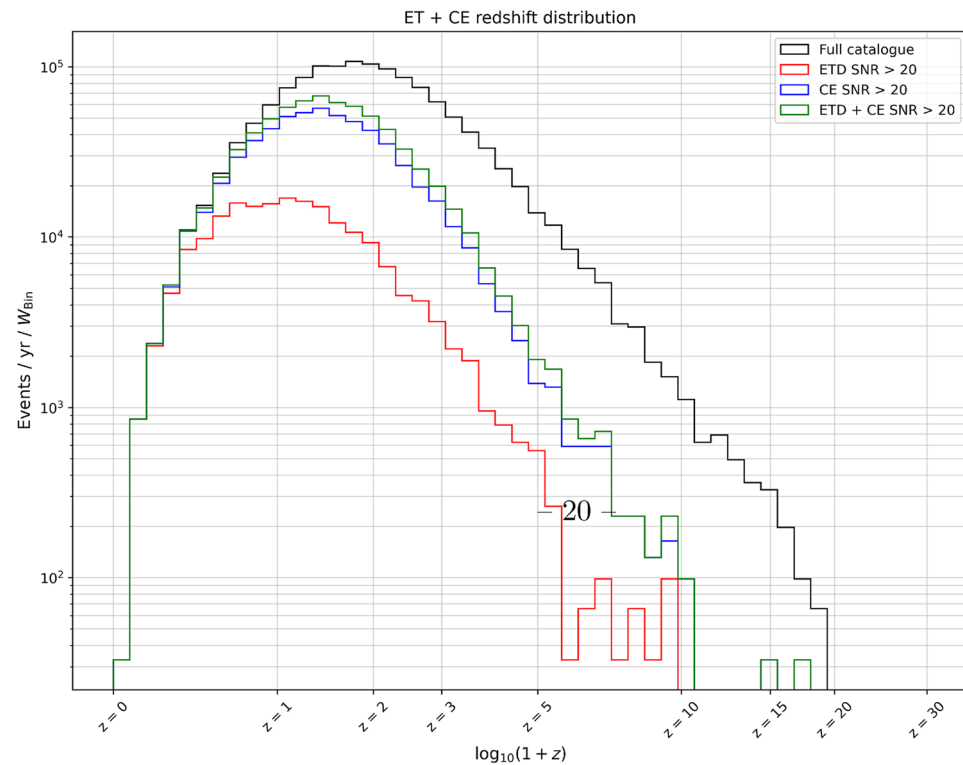
Figure 3. Total number of detected black hole mergers as a function of redshift, for ET, CE and the detector network ET+CE. Also shown is the intrinsic number of events that would be detected with an infinitely sensitive detector ("full catalogue").

With these assumptions, we generate mock catalogues of SOBHB mergers for an observation time of one year. In Fig. 3 we show the number of generated events ("full catalogue") and the ones detected with SNR > 20 for the two detectors separately and for a network ET+CE, as a function of redshift. In the case of the network we define an event *detectable* if it is detected with SNR larger than 20 in both detectors. We can note that at low redshift the difference between the two detectors is rather small, while starting from $z \sim 1$ CE is able to detect more events. However, when the network ET+CE is considered, essentially all the events up to $z \sim 1.5$ are detectable. For comparison, at the present LIGO/Virgo sensitivity, the number of detected BBH events with SNR > 20 is around four[13].

We then show in Fig. 4 the distribution of events per year as a function of the detector-frame total mass. Note that the distribution of events shows a double peak structure, which reflects the power-law+peak mass intrinsic
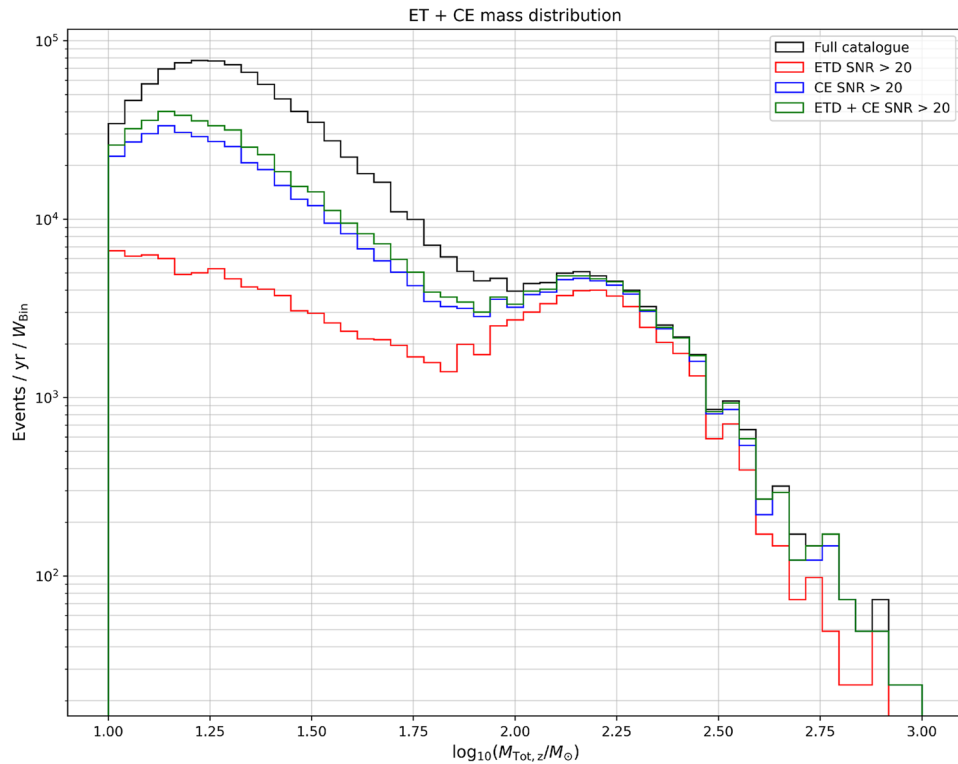
Figure 4. Total number of detected black hole mergers as a function the detector frame total mass, for ET, CE and the detector network ET+CE.

mass distribution adopted in this analysis. We can see that both ET and CE can detect a large number of GW sources with large masses. Some of these may also be observable (during their inspiral phase) in LISA[57], which would greatly enhance the possibility to use these sources to test General Relativity[58,59] or to detect interactions with the surrounding astrophysical environment[60,61] (even if undetected as resolved events, these SOBHBs may also appear in LISA as a stochastic background[50,62,63]).

In order to assess the accuracy with which the two detectors can estimate SOBHB parameters, we use a Fisher matrix analysis[43,64–66]. The latter is computationally efficient and can be run on thousand of sources, while being accurate only in the limit of high SNR[43]. The Fisher matrix Γ for the signal h has the following elements[43]

$$\Gamma_{ij} = \left(\frac{\partial h}{\partial \theta^i} \middle| \frac{\partial h}{\partial \theta^j} \right), \tag{2.6}$$

where we are using the noise weighted inner product of eq. (2.4) and θ_i is the vector of source parameters. The derivatives with respect to all the parameters are computed analytically, except for the two masses m_1, m_2 and the spin parameters for which we use a fourth order finite difference scheme with Richardson extrapolation to vanishing step. Tests of convergence and robustness are performed on the fly trough our code. From the Fisher matrix we can build the covariance matrix Σ by taking its inverse, $\Sigma = \Gamma^{-1}$. In order to stabilize this numerical operation, we condition the parameters which are likely to have the lowest information *i.e.* the initial phase ϕ_0, the sky localization parameters θ and ϕ, the inclination ι and the phase ψ. In practice, this corresponds to adding a small number, which we set to be $\epsilon = 10^{-10}$, on the diagonal entries of the FIM corresponding to possibly poorly constrained parameters. This is equivalent to assuming a loose Gaussian prior with variance $1/\epsilon$ on those parameters. We have also tested that our choice of prior does not affect the parameter reconstruction.

The estimated statistical error on a parameter $\Delta\theta_i$ is then computed by extracting the corresponding diagonal element of the covariance matrix, while the error on combinations of the parameters is computed by performing standard error propagation.

In our analysis we focus in particular on the error on the following parameters

- error on the chirp mass $\Delta\mathcal{M}_{c,z}$, where $\mathcal{M}_{c,z} = (m_1 m_2)^{3/5}/(m_1 + m_2)^{1/5}$;
- error on the symmetric mass ratio $\Delta\eta$, where $\eta = (m_1 m_2)/(m_1 + m_2)^2$;
- error on the sky location, related to the errors on the θ and ϕ angles by the relation[43,67–69]

$$\Delta\Omega = 2\pi \sin\theta \sqrt{(\Delta\theta\Delta\phi)^2 - (\Sigma^{\theta\phi})^2} \ ;$$

- error on the luminosity distance Δd_L.

- error on the two dimensionless spins $\Delta \chi_1$ and $\Delta \chi_2$;
- error on the inclination angle $\Delta \iota$.

In what follows, we will also compare the statistical error on d_L with the systematic error arising from weak lensing, which we compute by using the fitting formula of[33] (used also in[70] for LISA analyses):

$$\sigma_{lens}(z) = d_L(z) \times 0.066 \left(\frac{1 - (1+z)^{-0.25}}{0.25} \right)^{1.8}. \tag{2.7}$$

Parameter estimation

As shown in the previous section, the CE detector allows for a larger number of detected sources, compared to ET. This can be also seen in Fig. 5, where we plot the distribution of the events detected in one year, for ET and CE separately and for them working as a network. We can note again that CE has a slightly better ability to detect BBH sources at higher redshift; for ET it is expected that a large number of detected sources will be around $z \sim 1$, while for CE the maximum is at slightly larger redshift.

In Fig. 6 we also show the distribution of SNR for the detected binaries. One can see that a large number of events will have an SNR above 50. This is consistent with[71], confirming that ET and CE will be more sensitive than currently operating ground-based and future space-based detectors when it comes to detecting SOBHBs. As an example, in Fig. 7 we also show the distribution of source-frame mass and redshift for our simulated binaries (for one realization of the universe), together with the SNR (color coded), for the network ET+CE. One can see that the distribution in mass qualitatively follows the shape of the power-law+peak mass function, while the distribution of events in redshift has a maximum at $z \sim 2$. As expected, the SNR is larger for closer and more massive objects.

We will now compare the parameter estimation capabilities of ET and CE, which are an important metric to assess the relative performance of different detector designs. As an example, in Fig. 12 we show the Fisher matrix posteriors for one of the loudest BH binary system (with $\mathrm{SNR_{ET}} = 607, \mathrm{SNR_{CE}} = 596$) in a realization of our population, i.e. one with $d_L \simeq 0.57$ Gpc, $m_1 \simeq 38.28 M_\odot, m_2 \simeq 28.18 M_\odot, \tau_c \simeq 0.06$ yrs, $\phi_0 \simeq 3.74, \theta \simeq 0.92$, $\phi \simeq 0.05, \iota \simeq 1.67, \psi \simeq 1.16, S_1 \simeq 0.49, S_2 \simeq 0.40, \cos(\theta_1) \simeq 0.60, \cos(\theta_2) \simeq 0.61$, firstly comparing ET with CE and then combining the two detectors. As expected, CE, having two detectors at different locations, allows for estimating the extrinsic parameters (e.g. d_L and sky position) more precisely. This is of course due to the possibility of "triangulating" the sources in the sky. We show this also in Fig. 8, where we plot the projected error on the sky localization, luminosity distance and inclination for the whole SOBHB population. We can see that the two L-shaped CE detectors allow for a better determination of the sky position compared to the single ET triangular detector. However, in both cases we can reach a resolution of order $5 - 10 \deg^2$ for a quite large number of detected events. The combination of the two allows to reach accurate angular resolution up to percent level. On the other hand, the difference on the luminosity distance error is not so large, even if CE allows a good estimation for a larger number of events. A similar behavior holds also for the inclination angle.

To be more quantitative, in Table 1 we have reported the number of sources that can be localized in the sky within 10, 1 and 0.1 square degrees, for the two detectors and for the network at low (i.e., $z < 2$) and high (i.e., $z > 2$) redshift, for one year of observation. This information is crucial to understand how many detections can be useful for cosmography and for cross-correlation with galaxy surveys[72]. For comparison, we note that a 10 deg^2 error box is the field of view of SKA[73] or Vera Rubin Observatory (LSST)[74]. One can see that the difference in localization power between ET or CE alone compared to their combination is quite significant both at low and high redshift.

We have also estimated the percentage of events that can be detected with relative errors on the luminosity distance of 20%, 10% and 5% for redshift below and above $z = 2$, including the systematic error due to weak lensing. From Table 2, one can see that at low redshift a reasonable number of events are detectable with a 20% accuracy in the three configurations (ET, CE and ET+CE). However, as more stringent requirements on the determination of the luminosity distance are considered, one can clearly see the benefit of having a network of detectors. Note that at high redshift, however, no events are detectable with accuracy below 5% and just a few with 10% accuracy. An explanation for this limitation can be obtained from the plot in Fig. 9, where we have compared for the network ET+CE the statistical error on the distance with the weak lensing contribution, which becomes dominant at high z.

The parameter estimation results for the intrinsic parameters (i.e., detector-frame chirp mass, symmetric mass ratio and spins) are shown in Fig. 10. As can be seen, the impact of the detector choice is less significant than for the extrinsic parameters. In more detail, with both detectors considered in this work, the chirp mass is always estimated to sub-percent error or better, with a slightly better error given by CE. The symmetric mass ratio and the spins are estimated to within 1% or better for most detected events, and for the symmetric mass ratio a large fraction of sources are expected to be measured even with sub-percent error. Finally in Fig. 11 we plot the projected relative error on the difference between the two spins.

In our analysis we have not neglected correlations between the parameters; in fact, in Fig. 12 it can be noticed that there are some correlations among some parameters; for instance it is manifest that there is a degeneracy $\theta - \phi$. Two important remarks about the correlation are the followings: i) to produce Fig. 12, we have chosen one of the loudest events (i.e., SNR $\simeq 600$) which of course translate in tighter errors on several parameters; ii) in our analysis we have included higher order modes in the waveform which help in reducing some degeneracies.
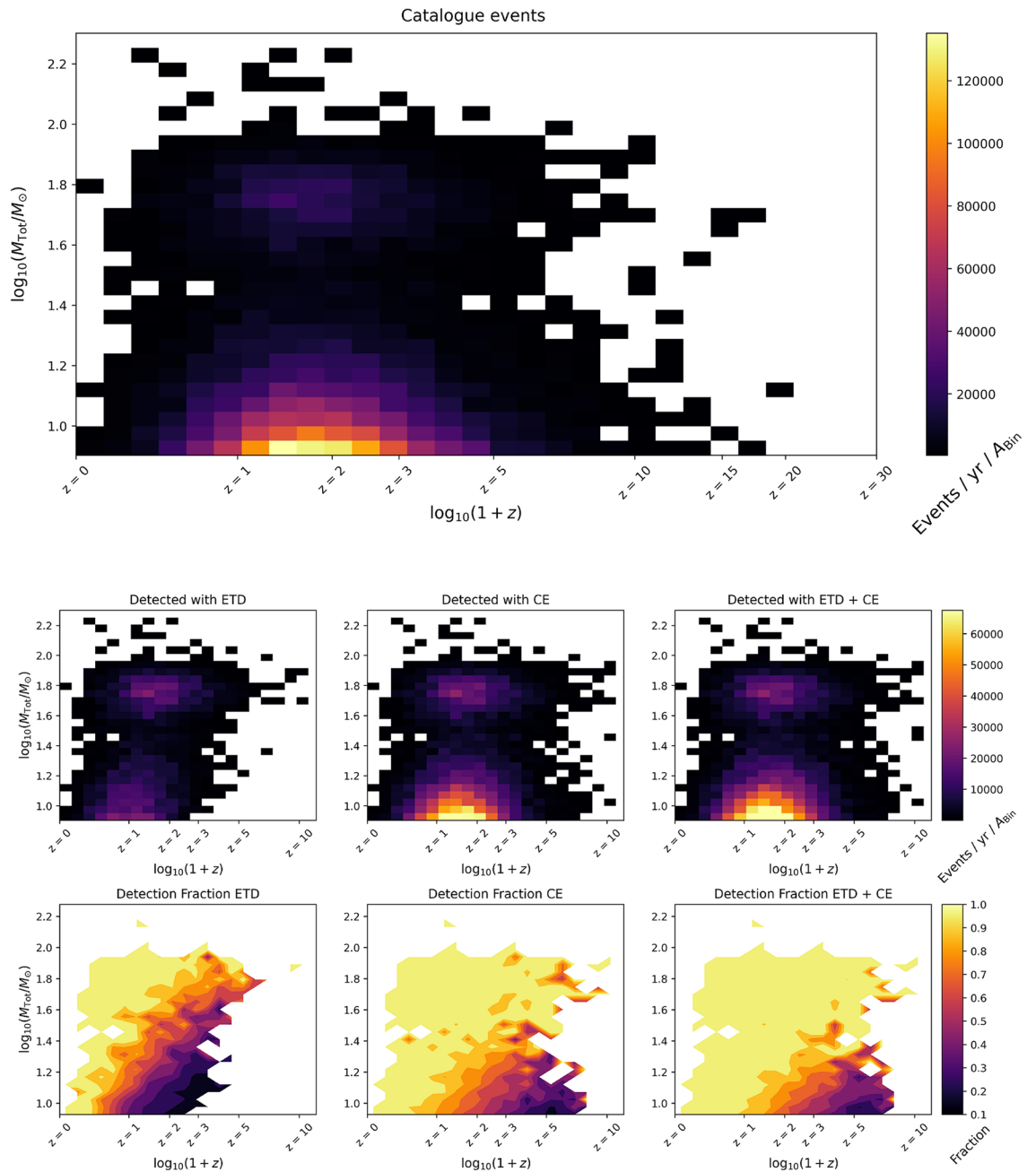
Figure 5. Fraction of the astrophysical population of black hole binaries that is detected, with the ET, CE or the network ET+CE.

Conclusions

Among the most interesting proposals to improve the sensitivity of current ground-based GW interferometers there are the ET and CE detectors. These interferometers will be characterized by longer arm-lengths and an order of magnitude better sensitivity compared to the LIGO/Virgo/KAGRA detectors. They are currently planned to have a triangular and L-shape geometry, respectively. With these characteristics, they will offer the possibility of exploring our universe up to high redshift and to detect a large number of GW sources, shedding light on the population properties of compact objects through the dark age of our universe. In this paper, we have studied the detectability and parameter estimation capabilities of ET and CE, considering them both independently or in a network. We have developed synthetic catalogues for one of the primary targets of ET and CE – SOBHBs – accounting for the latest LIGO/Virgo constraints on the population properties. We have used a redshift-dependent merger rate and a power-law plus peak mass function.
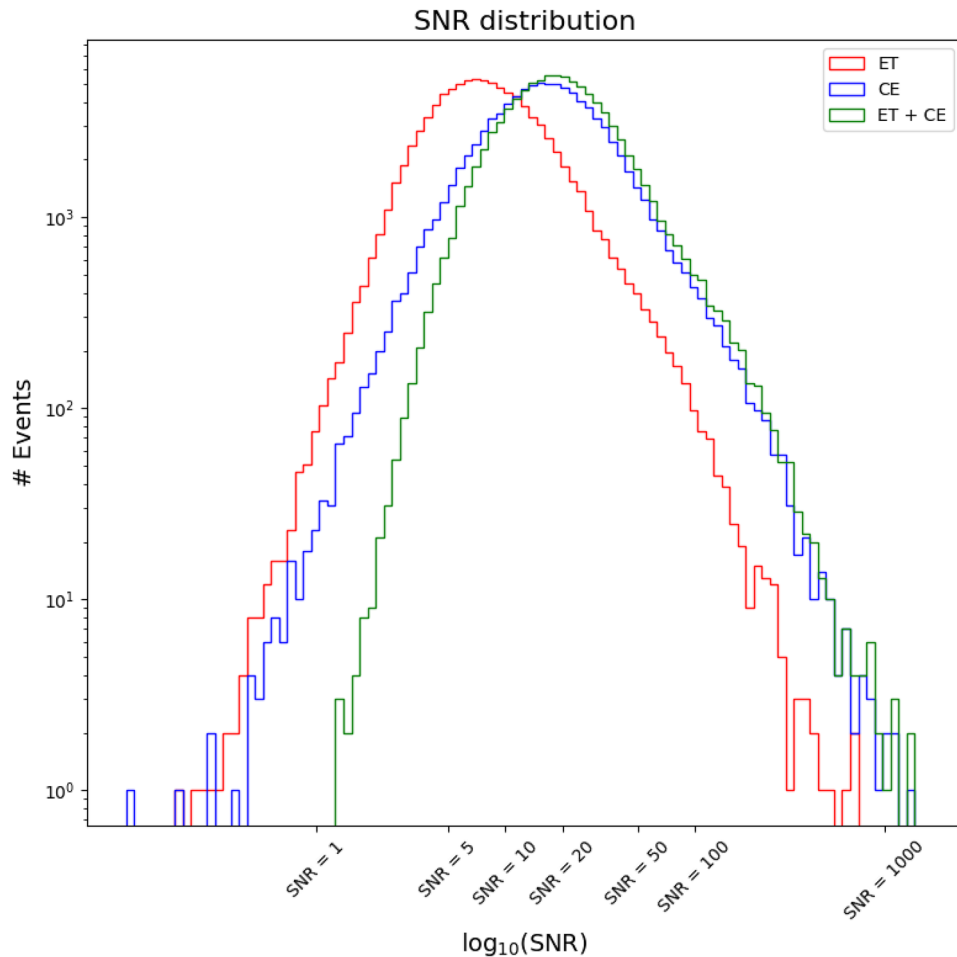
Figure 6. SNR distribution for ET, CE, and the network ET+CE.

We have first estimated the number of detectable events with the two detectors and with the network, and we have found that both options offer the chance to detect a large number of SOBHBs up to redshift $z \sim 5 - 6$. When the two instruments are considered in a network, almost all the SOBHBs up to $z \sim 1.5$ can be individually detected. ET and CE will also detect these systems with a high SNR, which will help in determining the source parameters.

Using a Fisher matrix analysis, we have then estimated the error on the intrinsic and extrinsic source parameters. As expected, the two L-shaped CE interferometers have better sky localization capabilities, while the errors on the luminosity distance Δd_L and the inclination angle $\Delta \iota$ are comparable. We have also quantified the number of detectable events with given sky resolution ($\Delta \Omega < 10, 1, 0.1$ square degrees) at low and high redshift ($z < 2$ and $z > 2$). We have found that the network ET+CE will have a good angular resolution (better than 10 square degrees) up to $z \lesssim$ 3-4, which may allow for cross-correlating SOBHB events with galaxy surveys such as SKA or the Vera Rubin Observatory. The number of detectable events with good angular resolution, however, drastically decreases at higher z. A similar analysis for the luminosity distance shows that the number of events with fixed error (better than 20%, 10% and 5%) is always larger for the ET detector. Moreover, the network ET+CE allows for a very accurate (10% or better) measurement of the luminosity distance for almost half of the detected events. At high redshift, especially at $z \gtrsim 3$, the error on the distance increases due to weak lensing. As for the intrinsic source parameters, the error on the chirp mass is slightly better for CE. As for the symmetric mass ratio and the spins, errors are projected to be comparable for ET and CE, with CE allowing an accurate estimation for a larger number of events. When a network of the two detectors is considered, the errors further improve down to sub-percent levels.

One limitation of the current work consists in the assumption of non-overlapping signals. The event rate that we find for SOBHBs implies a detection every few hours, which would imply the possibility to have many of them overlapping. On the other hand we did not include binaries of NSs, which are also a prominent source for ET and CE. We leave the inclusion of NS sources and overlapping signals for future works.
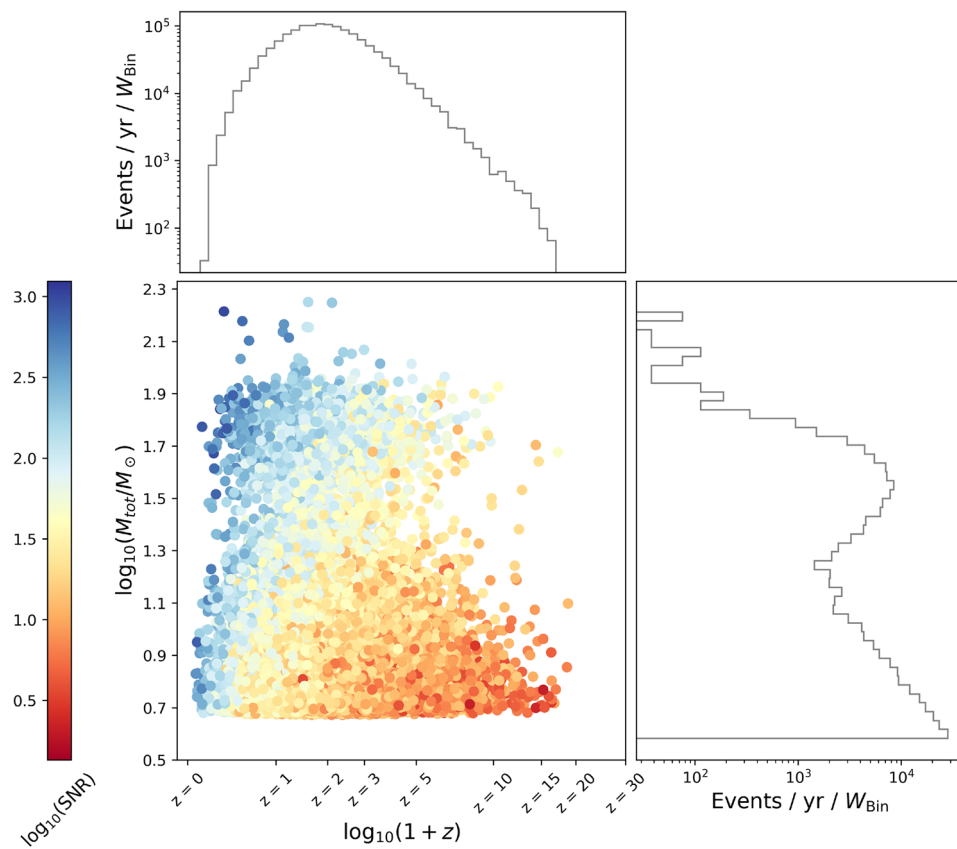
Figure 7. The distribution of source-frame mass and redshift for one universe realization, together with the SNR (color coded), for the network ET+CE.
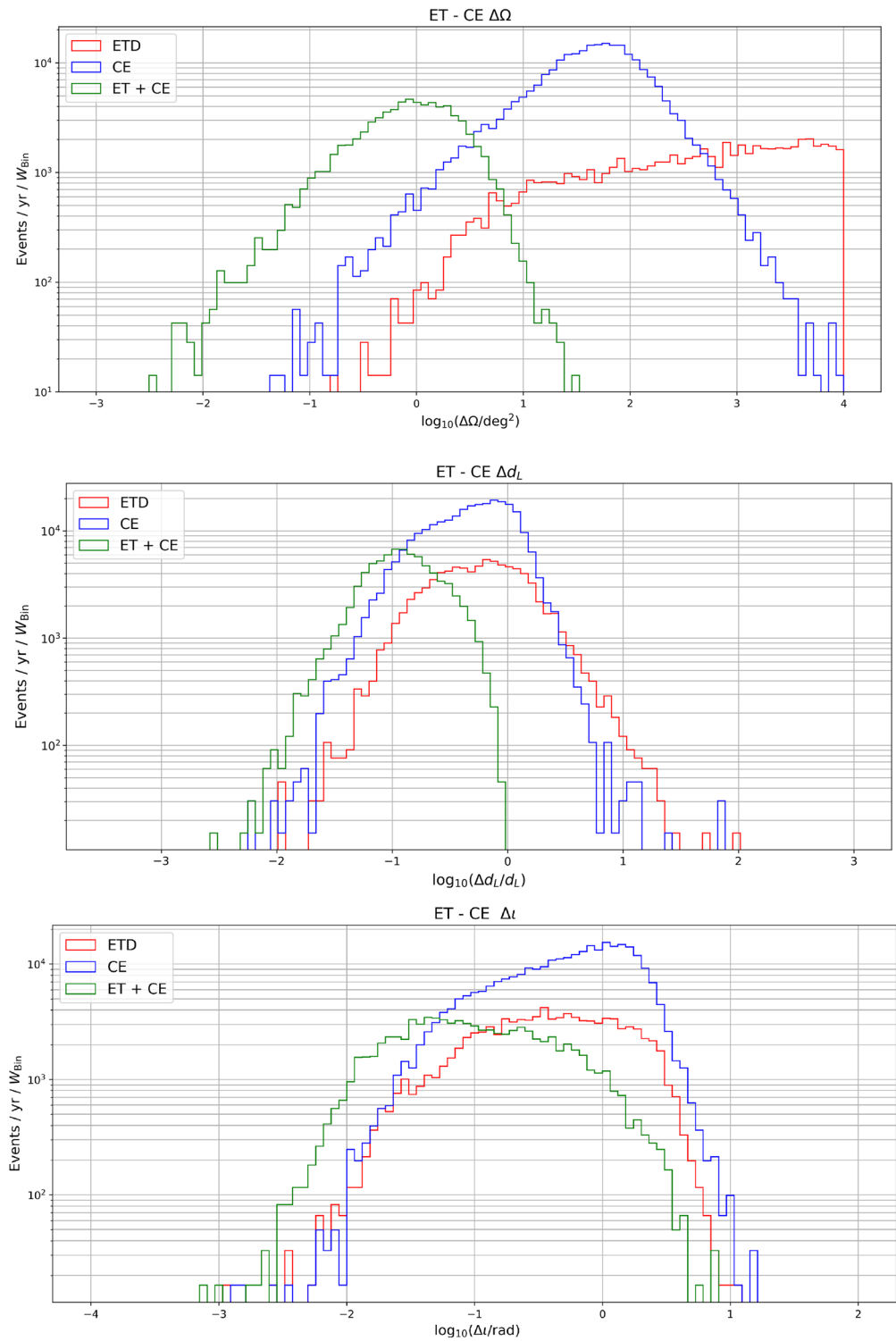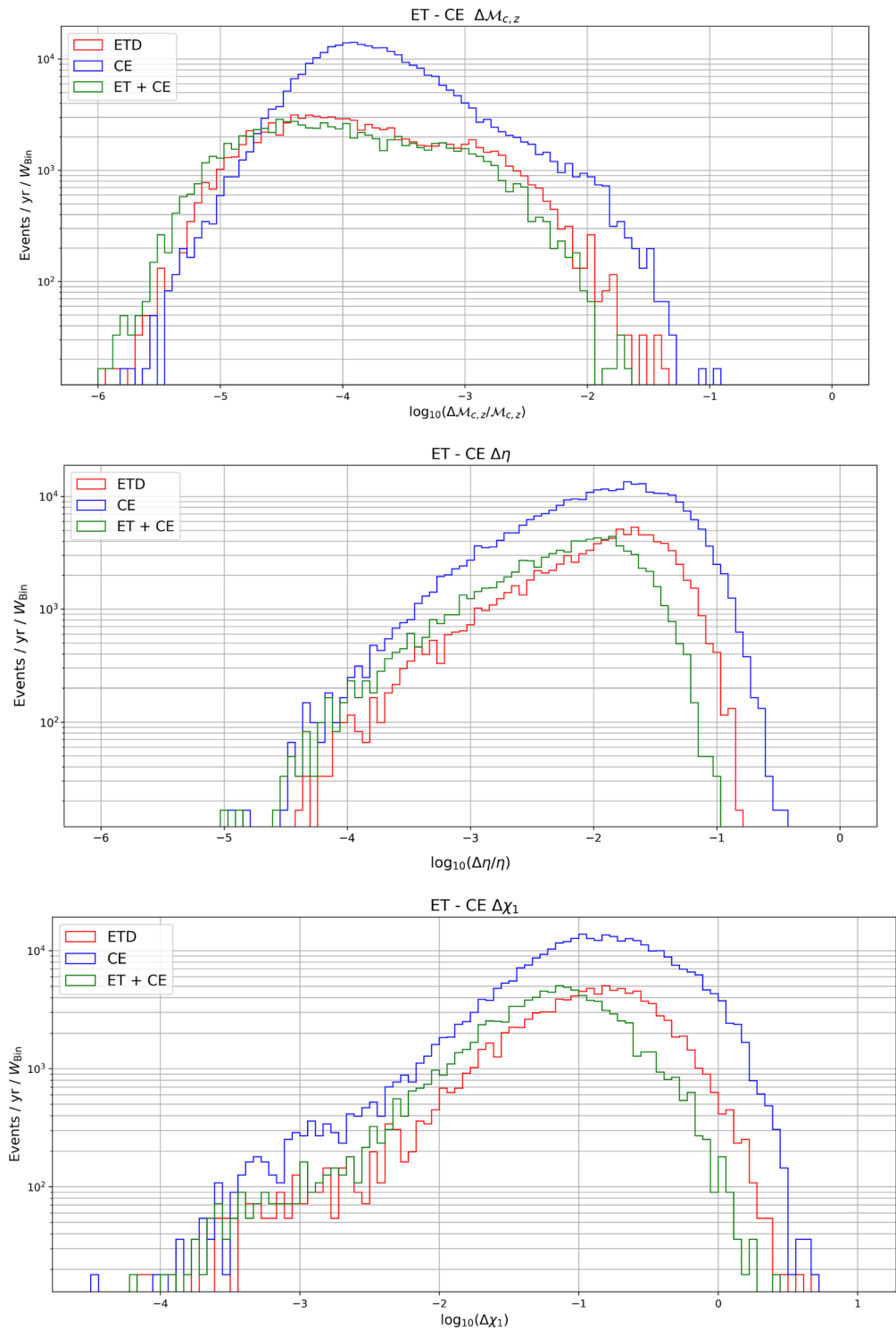
Figure 8. Projected errors on the measurements of the sky position, luminosity distance and inclination, for the detected events (SNR > 20) in one year for ET, CE and a network ET+CE.

	ET	CE	ET + CE
z < 2			
#events	4769	13302	4372
$\Delta\Omega < 10$	6.5%	16%	99.8%
$\Delta\Omega < 1$	0.44%	1.62%	59.7%
$\Delta\Omega < 0.1$	0.%	0.05%	5.9%
z > 2			
#events	872	4388	805
$\Delta\Omega < 10$	4.47%	5.4%	98%
$\Delta\Omega < 1$	0%	0.2%	26.5%
$\Delta\Omega < 0.1$	0%	0%	0%

Table 1. Percentage of events that can be detected with relative errors within 10, 1 and 0.1 square degrees on the sky localization angle. The left table refers to redshifts below $z = 2$, while right one refers to redshifts above $z = 2$.

|	ET	CE	ET + CE
z < 2			
#events	4769	13302	4372
$\Delta d_L < 20\%$	16%	21%	75%
$\Delta d_L < 10\%$	4.4%	7%	45%
$\Delta d_L < 5\%$	0.77%	1.3%	13%
z > 2			
#events	872	4388	805
$\Delta d_L < 20\%$	11%	11.3%	76%
$\Delta d_L < 10\%$	0%	0.3%	8.3%
$\Delta d_L < 5\%$	0%	0%	0%

Table 2. Percentage of events that can be detected with relative errors on the luminosity distance of 20%, 10% and 5%. The left table refers to redshifts below $z = 2$, while the right one refers to redshifts above $z = 2$.

Figure 9. Projected errors on the measurements of the intrinsic parameters, i.e. the (detector-frame) chirp mass, symmetric mass ratio and spins.
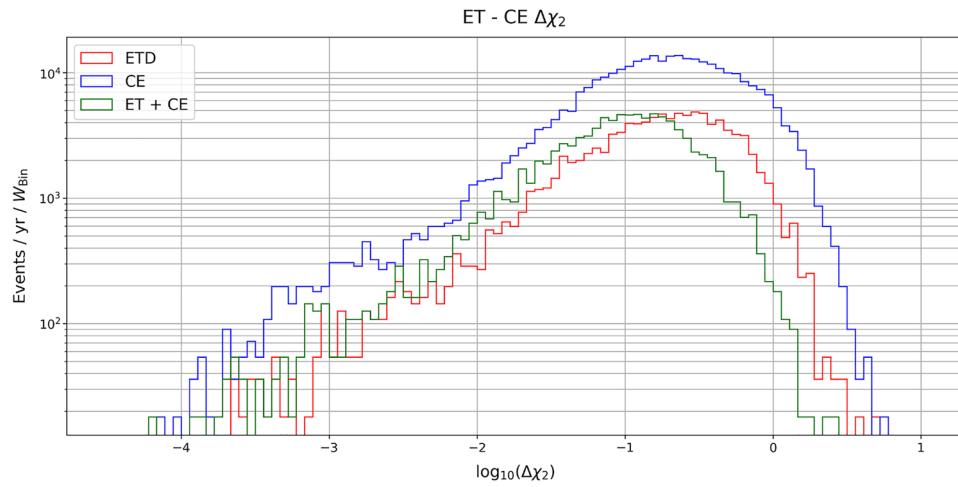
Figure 10. Projected relative error on the second spin.
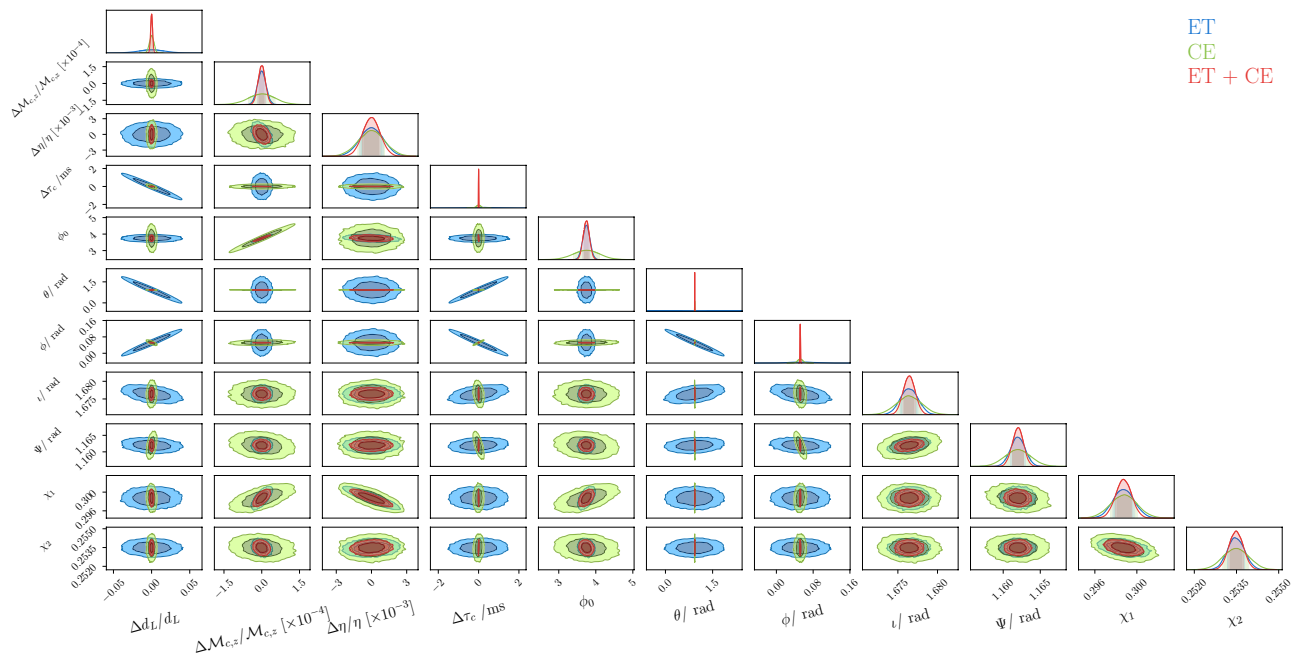
Figure 11. Fisher-matrix posteriors for ET, CE and the network ET+CE, for one of the loudest system (i.e., $\text{SNR}_{\text{ET}} = 607$, $\text{SNR}_{\text{CE}} = 596$) in one of our realizations of the universe, i.e. one with $d_L \simeq 0.57$ Gpc, $m_1 \simeq 38.28 M_\odot$, $m_2 \simeq 28.18 M_\odot$, $\tau_c \simeq 0.06$ yrs, $\phi_0 \simeq 3.74$, $\theta \simeq 0.92$, $\phi \simeq 0.05$, $\iota \simeq 1.67$, $\psi \simeq 1.16$, $S_1 \simeq 0.49$, $S_2 \simeq 0.40$, $\cos(\theta_1) \simeq 0.60$, $\cos(\theta_2) \simeq 0.61$. For practical reasons, the central value of τ_c here is set to zero. The credible levels in the plot represent the 1 and 2σ regions for the astrophysical parameters.
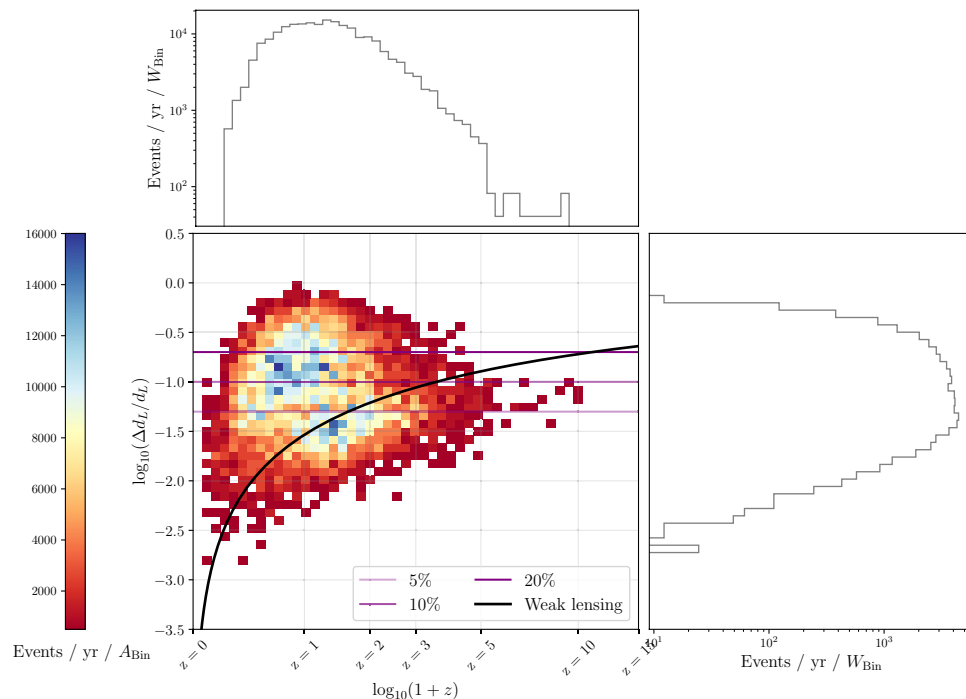
Figure 12. Projected relative error on the luminosity distance coming from the weak lensing compared with the statistical error on the distance determination for the network ET+CE.

Data availability

The datasets used and/or analysed during the current study available from the corresponding author on reasonable request.

References

1. Punturo, M. *et al.* The Einstein telescope: A third-generation gravitational wave observatory. *Class. Quant. Grav.* **27**, 194002. https://doi.org/10.1088/0264-9381/27/19/194002 (2010).
2. Hild, S. *et al.* Sensitivity studies for third-generation gravitational wave observatories. *Class. Quant. Grav.* **28**, 094013. https://doi.org/10.1088/0264-9381/28/9/094013 (2011) [arXiv:1012.0908].
3. shape LIGO Scientific collaboration. Exploring the sensitivity of next generation gravitational wave detectors. *Class. Quant. Grav.* **34**, 044001. https://doi.org/10.1088/1361-6382/aa51f4 (2017).
4. LISA collaboration, *Laser Interferometer Space Antenna*, arXiv:1702.00786.
5. shape LIGO Scientific. Virgo collaboration, observation of gravitational waves from a binary black hole merger. *Phys. Rev. Lett.* **116**, 061102. https://doi.org/10.1103/PhysRevLett.116.061102 (2016).
6. shape LIGO Scientific. Virgo collaboration, GWTC-1: A gravitational-wave transient catalog of compact binary mergers observed by LIGO and virgo during the first and second observing runs. *Phys. Rev. X* **9**, 031040. https://doi.org/10.1103/PhysRevX.9.031040 (2019).
7. shape LIGO Scientific. Virgo collaboration, GWTC-2: Compact binary coalescences observed by LIGO and virgo during the first half of the third observing run. *Phys. Rev. X* **11**, 021053. https://doi.org/10.1103/PhysRevX.11.021053 (2021).
8. LIGO Scientific, VIRGO, KAGRA collaboration, *GWTC-3: Compact binary coalescences observed by LIGO and virgo during the second part of the third observing run*, arXiv:2111.03606.
9. Regimbau, T. *et al.* A mock data challenge for the einstein gravitational-wave telescope. *Phys. Rev. D* **86**, 122001. https://doi.org/10.1103/PhysRevD.86.122001 (2012).
10. Belgacem, E. *et al.* Cosmology and dark energy from joint gravitational wave-GRB observations. *JCAP* **08**, 015. https://doi.org/10.1088/1475-7516/2019/08/015 (2019).
11. Sathyaprakash, B. S. et al. *Cosmology and the Early Universe*, arXiv:1903.09260.
12. Maggiore, M. *et al.* Science Case for the Einstein Telescope. *JCAP* **03**, 050. https://doi.org/10.1088/1475-7516/2020/03/050 (2020).
13. LIGO Scientific, VIRGO, KAGRA collaboration, The population of merging compact binaries inferred using gravitational waves through GWTC-3, arXiv:2111.03634.
14. García-Quirós, C. *et al.* Multimode frequency-domain model for the gravitational wave signal from nonprecessing black-hole binaries. *Phys. Rev. D* **102**, 064002. https://doi.org/10.1103/PhysRevD.102.064002 (2020).
15. Bird, S. *et al.* Did LIGO detect dark matter?. *Phys. Rev. Lett.* **116**, 201301. https://doi.org/10.1103/PhysRevLett.116.201301 (2016).
16. De Luca, V., Franciolini, G., Pani, P. & Riotto, A. Primordial Black Holes Confront LIGO/Virgo data: Current situation. *JCAP* **06**, 044. https://doi.org/10.1088/1475-7516/2020/06/044 (2020).
17. Clesse, S. & García-Bellido, J. The clustering of massive Primordial Black Holes as Dark Matter: measuring their mass distribution with Advanced LIGO. *Phys. Dark Univ.* **15**, 142. https://doi.org/10.1016/j.dark.2016.10.002 (2017).
18. Domcke, V., Muia, F., Pieroni, M. & Witkowski, L. T. PBH dark matter from axion inflation. *JCAP* **07**, 048. https://doi.org/10.1088/1475-7516/2017/07/048 (2017).

19. Bartolo, N. *et al.* Gravitational wave anisotropies from primordial black holes. *JCAP* **02**, 028. https://doi.org/10.1088/1475-7516/2020/02/028 (2020).
20. Laguna, P., Larson, S. L., Spergel, D. & Yunes, N. Integrated Sachs-Wolfe Effect for Gravitational Radiation. *Astrophys. J. Lett.* **715**, L12. https://doi.org/10.1088/2041-8205/715/1/L12 (2010).
21. Jeong, D. & Schmidt, F. Large-Scale Structure with Gravitational Waves I: Galaxy Clustering. *Phys. Rev. D* **86**, 083512. https://doi.org/10.1103/PhysRevD.86.083512 (2012).
22. Camera, S. & Nishizawa, A. Beyond Concordance Cosmology with Magnification of Gravitational-Wave Standard Sirens. *Phys. Rev. Lett.* **110**, 151103. https://doi.org/10.1103/PhysRevLett.110.151103 (2013).
23. Oguri, M. Measuring the distance-redshift relation with the cross-correlation of gravitational wave standard sirens and galaxies. *Phys. Rev. D* **93**, 083511. https://doi.org/10.1103/PhysRevD.93.083511 (2016).
24. Raccanelli, A., Kovetz, E. D., Bird, S., Cholis, I. & Munoz, J. B. Determining the progenitors of merging black-hole binaries. *Phys. Rev. D* **94**, 023516. https://doi.org/10.1103/PhysRevD.94.023516 (2016).
25. Scelfo, G., Bellomo, N., Raccanelli, A., Matarrese, S. & Verde, L. GW×LSS: chasing the progenitors of merging binary black holes. *JCAP* **09**, 039. https://doi.org/10.1088/1475-7516/2018/09/039 (2018).
26. Scelfo, G., Boco, L., Lapi, A. & Viel, M. Exploring galaxies-gravitational waves cross-correlations as an astrophysical probe. *JCAP* **10**, 045. https://doi.org/10.1088/1475-7516/2020/10/045 (2020).
27. Adhikari, S., Fishbach, M., Holz, D. E., Wechsler, R. H. & Fang, Z. The Binary-Host Connection: Astrophysics of Gravitational-Wave Binaries from Host Galaxy Properties. *Astrophys. J.* **905**, 21. https://doi.org/10.3847/1538-4357/abbfb7 (2020).
28. Del Pozzo, W. Inference of the cosmological parameters from gravitational waves: application to second generation interferometers. *Phys. Rev. D* **86**, 043011. https://doi.org/10.1103/PhysRevD.86.043011 (2012).
29. Mukherjee, S. & Wandelt, B. D. Beyond the classical distance-redshift test: Cross-correlating redshift-free standard candles and sirens with redshift surveys, arXiv:1808.06615.
30. Libanore, S. *et al.* Gravitational Wave mergers as tracers of Large Scale Structures. *JCAP* **02**, 035. https://doi.org/10.1088/1475-7516/2021/02/035 (2021).
31. Libanore, S. *et al.* Clustering of Gravitational Wave and Supernovae events: a multitracer analysis in Luminosity Distance Space. *JCAP* **02**, 003. https://doi.org/10.1088/1475-7516/2022/02/003 (2022).
32. Holz, D. E. & Linder, E. V. Safety in numbers: Gravitational lensing degradation of the luminosity distance-redshift relation. *Astrophys. J.* **631**, 678. https://doi.org/10.1086/432085 (2005).
33. Hirata, C. M., Holz, D. E. & Cutler, C. Reducing the weak lensing noise for the gravitational wave Hubble diagram using the non-Gaussianity of the magnification distribution. *Phys. Rev. D* **81**, 124046. https://doi.org/10.1103/PhysRevD.81.124046 (2010).
34. Bertacca, D., Raccanelli, A., Bartolo, N. & Matarrese, S. Cosmological perturbation effects on gravitational-wave luminosity distance estimates. *Phys. Dark Univ.* **20**, 32. https://doi.org/10.1016/j.dark.2018.03.001 (2018).
35. Bertacca, D. *et al.* Projection effects on the observed angular spectrum of the astrophysical stochastic gravitational wave background. *Phys. Rev. D* **101**, 103513. https://doi.org/10.1103/PhysRevD.101.103513 (2020).
36. "Cosmic explorer sensitivity." https://cosmicexplorer.org/sensitivity.html.
37. http://www.et-gw.eu/index.php/etsensitivities.
38. Thrane, E. & Romano, J. D. Sensitivity curves for searches for gravitational-wave backgrounds. *Phys. Rev. D* **88**, 124032. https://doi.org/10.1103/PhysRevD.88.124032 (2013) [arXiv:1310.5300].
39. Caprini, C. *et al.* Reconstructing the spectral shape of a stochastic gravitational wave background with LISA. *JCAP* **11**, 017. https://doi.org/10.1088/1475-7516/2019/11/017 (2019).
40. Borhanian, S. & Sathyaprakash, B. S.: Listening to the Universe with Next Generation Ground-Based Gravitational-Wave Detectors, arXiv:2202.11048.
41. Nitz, A., Harry, I., Brown, D., Biwer, C. M., Willis, J. & Canton, T. D. et al. *gwastro/pycbc*, https://doi.org/10.5281/zenodo.5347736 (2021).
42. Maggiore, M. Gravitational wave experiments and early universe cosmology. *Phys. Rept.* **331**, 283. https://doi.org/10.1016/S0370-1573(99)00102-7 (2000).
43. Cutler, C. & Flanagan, E. E. Gravitational waves from merging compact binaries: How accurately can one extract the binary's parameters from the inspiral wave form?. *Phys. Rev. D* **49**, 2658. https://doi.org/10.1103/PhysRevD.49.2658 (1994).
44. Planck collaboration. Planck 2018 results. VI. Cosmological parameters. *Astron. Astrophys.* **641**(2020), A6. https://doi.org/10.1051/0004-6361/201833910 (2020).
45. Madau, P. & Dickinson, M. Cosmic Star Formation History. *Ann. Rev. Astron. Astrophys.* **52**, 415. https://doi.org/10.1146/annurev-astro-081811-125615 (2014).
46. Mapelli, M., Giacobbo, N., Ripamonti, E. & Spera, M. The cosmic merger rate of stellar black hole binaries from the Illustris simulation. *Mon. Not. R. Astron. Soc.* **472**, 2422. https://doi.org/10.1093/mnras/stx2123 (2017).
47. KAGRA, Virgo, LIGO Scientific collaboration. Upper limits on the isotropic gravitational-wave background from advanced LIGO and advanced Virgo's third observing run. *Phys. Rev. D* **104**, 022004. https://doi.org/10.1103/PhysRevD.104.022004 (2021).
48. Singh, N., Bulik, T., Belczynski, K. & Askar, A. Exploring compact binary populations with the Einstein Telescope, arXiv:2112.04058.
49. Flauger, R. *et al.* Improved reconstruction of a stochastic gravitational wave background with LISA. *JCAP* **01**, 059. https://doi.org/10.1088/1475-7516/2021/01/059 (2021).
50. Pieroni, M. & Barausse, E. Foreground cleaning and template-free stochastic background extraction for LISA, arXiv:2004.01135.
51. Boileau, G., Lamberts, A., Christensen, N., Cornish, N. J. & Meyer, R. Spectral separation of the stochastic gravitational-wave background for LISA in the context of a modulated Galactic foreground. *Mon. Not. Roy. Astron. Soc.* **508**, 803. https://doi.org/10.1093/mnras/stab2575 (2021).
52. Bellomo, N., Bertacca, D., Jenkins, A. C., Matarrese, S., Raccanelli, A. & Regimbau, T. et al. CLASS_GWB: robust modeling of the astrophysical gravitational wave background anisotropies, arXiv:2110.15059.
53. Santoliquido, F., Mapelli, M., Giacobbo, N., Bouffanais, Y. & Artale, M. C. The cosmic merger rate density of compact objects: impact of star formation, metallicity, initial mass function and binary evolution. *Mon. Not. Roy. Astron. Soc.* **502**, 4877. https://doi.org/10.1093/mnras/stab280 (2021).
54. Calore, F., Cuoco, A., Regimbau, T., Sachdev, S. & Serpico, P. D. Cross-correlating galaxy catalogs and gravitational waves: a tomographic approach. *Phys. Rev. Res.* **2**, 023314. https://doi.org/10.1103/PhysRevResearch.2.023314 (2020).
55. Belgacem, E., Dirian, Y., Foffa, S. & Maggiore, M. Modified gravitational-wave propagation and standard sirens. *Phys. Rev. D* **98**, 023510. https://doi.org/10.1103/PhysRevD.98.023510 (2018).
56. Mukherjee, S., Wandelt, B. D. & Silk, J. Probing the theory of gravity with gravitational lensing of gravitational waves and galaxy surveys. *Mon. Not. R. Astron. Soc.* **494**, 1956. https://doi.org/10.1093/mnras/staa827. (2020).
57. Sesana, A. Prospects for multiband gravitational-wave astronomy after GW150914. *Phys. Rev. Lett.* **116**, 231102. https://doi.org/10.1103/PhysRevLett.116.231102 (2016).
58. Barausse, E., Yunes, N. & Chamberlain, K. Theory-Agnostic Constraints on Black-Hole Dipole Radiation with Multiband Gravitational-Wave Astrophysics. *Phys. Rev. Lett.* **116**, 241104. https://doi.org/10.1103/PhysRevLett.116.241104 (2016).
59. Toubiana, A., Marsat, S., Barausse, E., Babak, S. & Baker, J. Tests of general relativity with stellar-mass black hole binaries observed by LISA. *Phys. Rev. D* **101**, 104038. https://doi.org/10.1103/PhysRevD.101.104038 (2020).

60. Caputo, A., Sberna, L., Toubiana, A., Babak, S., Barausse, E. & Marsat, S. et al. Gravitational-wave detection and parameter estimation for accreting black-hole binaries and their electromagnetic counterpart, arXiv:2001.03620.

61. Toubiana, A. *et al.* Detectable environmental effects in GW190521-like black-hole binaries with LISA. *Phys. Rev. Lett.* **126**, 101105. https://doi.org/10.1103/PhysRevLett.126.101105 (2021).

62. Karnesis, N., Babak, S., Pieroni, M., Cornish, N. & Littenberg, T. Characterization of the stochastic signal originating from compact binary populations as measured by LISA. *Phys. Rev. D* **104**, 043019. https://doi.org/10.1103/PhysRevD.104.043019 (2021).

63. Marcoccia, P. et al. In preparation, .

64. Vallisneri, M. Use and abuse of the Fisher information matrix in the assessment of gravitational-wave parameter-estimation prospects. *Phys. Rev. D* **77**, 042001. https://doi.org/10.1103/PhysRevD.77.042001 (2008).

65. Cho, H.-S & Lee, C.-H. Application of the effective Fisher matrix to the frequency domain inspiral waveforms. *Class. Quant. Grav.* **31**, 235009. https://doi.org/10.1088/0264-9381/31/23/235009 (2014).

66. Nitz, A. H. & Dal Canton, T. Pre-merger Localization of Compact-binary Mergers with Third-generation Observatories. *Astrophys. J. Lett.* **917**, L27. https://doi.org/10.3847/2041-8213/ac1a75 (2021).

67. Barack, L. & Cutler, C. LISA capture sources: Approximate waveforms, signal-to-noise ratios, and parameter estimation accuracy. *Phys. Rev. D* **69**, 082005. https://doi.org/10.1103/PhysRevD.69.082005 (2004).

68. Zhao, W. & Wen, L. Localization accuracy of compact binary coalescences detected by the third-generation gravitational-wave detectors and implication for cosmology. *Phys. Rev. D* **97**, 064031. https://doi.org/10.1103/PhysRevD.97.064031 (2018).

69. Yu, J., Wang, Y., Zhao, W. & Lu, Y. Hunting for the host galaxy groups of binary black holes and the application in constraining Hubble constant. *Mon. Not. Roy. Astron. Soc.* **498**, 1786. https://doi.org/10.1093/mnras/staa2465 (2020).

70. Tamanini, N. *et al.* Science with the space-based interferometer eLISA. III: Probing the expansion of the Universe using gravitational wave standard sirens. *JCAP* **04**, 002. https://doi.org/10.1088/1475-7516/2016/04/002 (2016).

71. Grimm, S. & Harms, J. Multiband gravitational wave parameter estimation: A study of future detectors, arXiv:2004.01434.

72. Sathyaprakash, B. S., Schutz, B. F. & Van Den Broeck, C. Cosmography with the Einstein Telescope. *Class. Quant. Grav.* **27**, 215006. https://doi.org/10.1088/0264-9381/27/21/215006 (2010).

73. "Square kilometre array (SKA) project." https://www.skatelescope.org/the-ska-project/.

74. "Rubin observatory system & LSST survey key numbers." https://www.lsst.org/scientists/keynumbers.

Acknowledgements

Author contributions

E.B. provided guidance on how to perform a Fisher matrix analysis and produce the astrophysical catalogues. He also contributed to the writing of all sections. M.P. coded up the astrophysical catalogue generation and the Fisher matrix analysis, and produced all figures. A.R. contributed to checking M.P.'s codes and provided advice on the E.T. design. He also led the writing of the paper.

Competing interests

The authors declare no competing interests.

Additional information

Correspondence and requests for materials should be addressed to M.P.

Reprints and permissions information is available at www.nature.com/reprints.

Publisher's note Springer Nature remains neutral with regard to jurisdictional claims in published maps and institutional affiliations.